Available online at www.sciencedirect.com
ScienceDirect
Polar Science 1 (2007) 73–83
http://ees.elsevier.com/polar/

Estimation of seasonal changes in the flow of Shirase Glacier using JERS-1/SAR image correlation

Kazuki Nakamura*, Koichiro Doi, Kazuo Shibuya

National Institute of Polar Research, Japan

Received 27 March 2007; revised 13 August 2007; accepted 13 September 2007
Available online 26 November 2007

Abstract

This paper presents estimates of detailed seasonal variations in ice-flow velocity for Shirase Glacier calculated using data obtained by Japanese Earth Resources Satellite-1 (JERS-1) synthetic aperture radar (SAR). We used 12 pairs of images (44-day repeat cycle) over the interval from 30 April 1996 to 1 July 1998 to estimate ice-flow fields using an image correlation method. Geometric registration was performed with reference to the RADARSAT Antarctic Mapping Project (RAMP) image dataset. Error analysis based on feature mismatch indicated an absolute error of ±0.30 km/a and relative error of ±0.04 km/a in the estimated flow velocity. The obtained ice-flow velocity increases rapidly from the upstream region (1.18 km/a) to the grounding line, where it becomes stagnant (2.32 km/a), before accelerating gradually to 2.62–2.82 km/a in the downstream region and then increasing to 3.05–3.50 km/a at the terminus of the floating ice tongue. The ice-flow velocities in the downstream region are highly variable, depending on both the distance from the grounding line and the observed epoch (season). Most of the obtained seasonal variations in ice-flow velocity at the floating ice tongue are within the range of the associated error estimate, but the annual difference between 1997 (3.11 km/a) and 1998 (3.50 km/a) is significant, reflecting a possible acceleration in the ice-flow velocity in association with the disappearance of the floating ice tongue between April and May of 1998. In terms of the summer–winter difference in averaged air temperature, the large difference recorded in 1997 (17.0 °C) relative to 1996 (13.9 °C) corresponds to a reduced ice-flow velocity in 1997 (approximately 0.20 km/a) relative to that in 1996 (approximately 0.30 km/a), indicating interactions between air, sea ice, and glacier flow in Lützow-Holm Bay.

Keywords: East Antarctica; Shirase Glacier; Ice flow; Seasonal change; Synthetic aperture radar (SAR)

1. Introduction

Estimating the flow velocities of ice streams in Antarctica is very important in understanding the mass balance of the ice sheet, as the discharge of ice mass is largely dependent on the velocity of ice streams. Ice-flow velocities in the area of the Shirase Glacier have been estimated in the past using several different methods. Ice flow at the floating ice tongue has been detected from the movement of icebergs recorded on aerial photographs taken in the 1960s and 1970s, yielding an estimated flow value of 2.5 km/a (Nakawo et al., 1978; Fujii, 1981). Recent satellite remote sensing data also indicate a flow velocity at the floating

* Corresponding author. Present address: National Institute of Advanced Industrial Science and Technology, Geologic Remote Sensing Research Group, AIST central 7, Higashi 1-1-1, Tsukuba, Ibaraki 305-8567, Japan. Tel.: +81 29 861 3619; fax: +81 29 861 3788.
E-mail address: nakamura-kazuki@aist.go.jp (K. Nakamura).

1873-9652/$ - see front matter © 2007 Elsevier B.V. and NIPR. All rights reserved.
doi:10.1016/j.polar.2007.09.002

ice tongue of 2.2 to 2.6 km/a (Pattyn and Derauw, 2002), with an estimated flow velocity at the grounding line of 2.3 km/a (Rignot, 2002). These results demonstrate that Shirase Glacier is one of the fastest-moving ice streams in Antarctica.

Previous studies have reported only the annual mean ice-flow velocity of Shirase Glacier; however, the flow velocity needs to be investigated in greater detail to precisely determine seasonal changes in the mass balance of the Antarctic ice-sheet. Microwave remote sensing data, and in particular synthetic aperture radar (SAR) data, are useful in this regard because of their all-weather observation capabilities and high spatial resolution (30−50 m).

Pattyn and Derauw (2002) and Rignot (2002) derived the above flow velocities using the interferometric SAR technique. Because complex SAR data decorrelate rapidly (within 10 days) over the ice-sheet and glacier area, application of the interferometric SAR technique is limited to images acquired over short time periods of around 3 days. This means that phase correlation cannot be achieved without data from the European Remote Sensing Satellite (ERS) tandem mission (1-day repeat cycle) or the ERS-1 ice mode operation (3-day repeat cycle). Given that both missions are limited in their operational schedule (4 months around Shirase Glacier and 14 months in total for a tandem mission; 7 months in total for an ice mode operation), seasonal variations cannot be detected using these archived ERS SAR data.

In contrast, the approach taken in matching the amplitudes of SAR images can be used in correlating scenes over a long time period, as shown by Wakabayashi and Nishio (2004). The present paper presents detailed estimates of ice-flow vectors for Shirase Glacier obtained using the SAR amplitude image-correlation method. This method can be applied to a long observation span (1996−1998 in the present study) and a long repeat cycle (44 days in the present study) for SAR data obtained by the Japanese Earth Resources Satellite-1 (JERS-1).

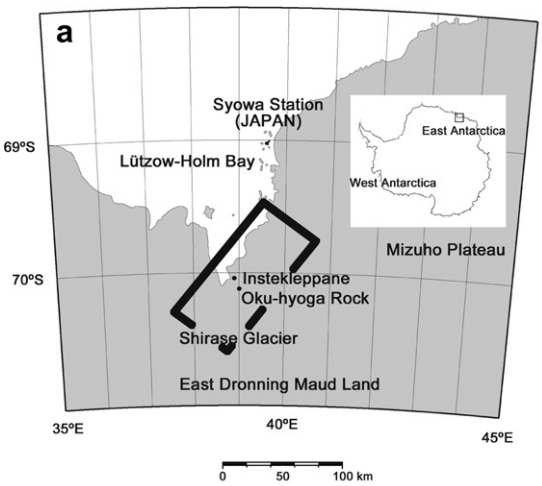

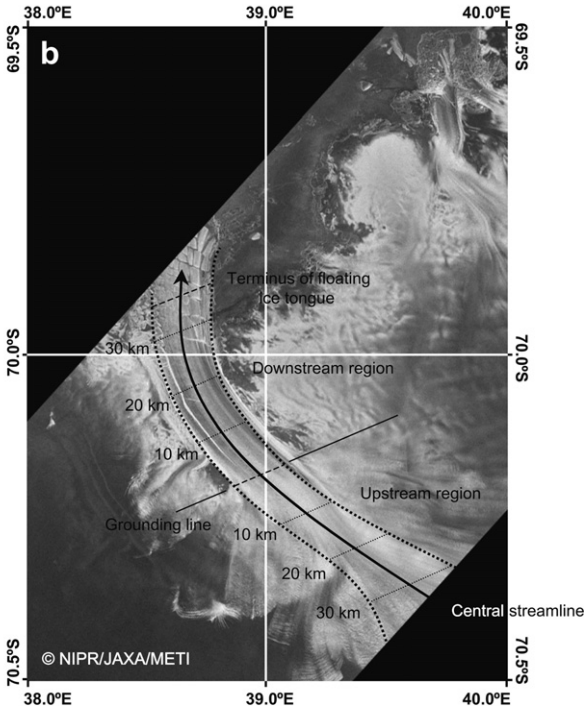

Fig. 1. (a) Map of Lützow-Holm Bay, East Antarctica. The black rectangle defines the area of Shirase Glacier analyzed in the present study. (b) Location of the grounding line (as determined by Yamanokuchi et al., 2005) overlain upon a JERS-1 SAR image taken on 30 April 1996. For further clarification of the extent of the upstream and downstream regions, see Fig. 5.

2. Shirase Glacier

The Shirase Glacier was named after the famous explorer Nobu Shirase, who attempted to become the first Japanese explorer to reach the South Pole. The Glacier is located approximately 150 km south of Syowa Station (Fig. 1(a)). The location of the grounding line shown in Fig. 1(b) was calculated based on the interferometric SAR technique (Yamanokuchi et al., 2005). For convenience, we divide the area into two regions relative to the grounding line: the upstream region extending to Dronning Maud Land (Mizuho Plateau), and the downstream region extending to Lützow-Holm Bay (Fig. 1(b)). Seasonal flow characteristics are discussed in terms of a representative central streamline (thick line in Fig. 1(b)).

The drainage basin of Shirase Glacier is the Mizuho Plateau area of Dronning Maud Land (Naruse, 1978; Mae and Naruse, 1978). The terminus of the ice stream of the glacier reaches Lützow-Holm Bay in the form of a floating ice tongue. Given that the floating ice tongue is surrounded by sea ice, the glacier mass has no direct outlet from Lützow-Holm Bay; instead, the elongated ice tongue is known to periodically disappear at intervals of approximately 10 years (e.g., Nishio, 1990), although the details of its outlet mechanism remain unknown.

Ushio et al. (2006) recently proposed a qualitative explanation of the outlet mechanism: at times of the disintegration of the sea ice surrounding the floating ice tongue, the terminus of the tongue fragments into icebergs that flow northward. Thus, the behavior of the floating ice tongue must be related to the stability of conditions in the sea-ice region of Lützow-Holm Bay.

3. JERS-1 SAR data

The JERS-1 satellite was launched on 11 February 1992 by the National Space Development Agency of Japan (NASDA; since reorganized as the Japan Aerospace Exploration Agency: JAXA). The onboard L-band SAR (wavelength: 23.5 cm) observes the Earth's surface from an altitude of 568 km with a repeat period of 44 days.

JERS-1 SAR intensively observed Shirase Glacier and its surrounding region from 1996 to 1998; these data were archived by the National Institute of Polar Research (NIPR) in collaboration with NASDA/JAXA. It is possible to estimate the displacement of a given point upon Shirase Glacier at 44-day intervals using the archived SAR data. Table 1 summarizes the SAR observation dates used in this study. The interval between epoch (1) and (2) is 44 days, providing good correlation between the two SAR scenes. Likewise, a good correlation was achieved between epochs (2) and (3), and so on; however, the interval between epochs (7) and (8) was 176 days, meaning that changed surface scattering characteristics between the two images give rise to a poor correlation. We used a total of 12 SAR image pairs ((a) through (l) in Table 1) to cover 2–3 seasons with the aim of detecting seasonal variations in the flow characteristics of Shirase Glacier.

Table 1
List of the JERS-1 SAR data used in the present analysis

(1) 30 Apr 1996 (a)	(8) 14 Jul 1997 (g)	(11) 06 Jan 1998 (i)
(2) 13 Jun 1996 (b)	(9) 27 Aug 1997 (h)	(12) 19 Feb 1998 (j)
(3) 27 Jul 1996 (c)	(10) 10 Oct 1997	(13) 04 Apr 1998 (k)
(4) 09 Sep 1996 (d)		(14) 18 May 1998 (l)
(5) 23 Oct 1996 (e)		(15) 01 Jul 1998
(6) 06 Dec 1996 (f)		
(7) 19 Jan 1997		

The numbering used in this table corresponds to the SAR observation dates in Fig. 2.

4. Data analysis

4.1. SAR data processing

The application of an image correlation method in estimating the ice-flow vector requires accurately co-registered SAR images. We first generated single-look complex (SLC) images from JERS-1 raw data using the common routine of the GAMMA SAR Processor developed by GAMMA Remote Sensing Research and Consulting AG, Switzerland. From the generated SLC images, we precisely estimated the range and azimuth offsets to sub-pixel accuracy, and accurately co-registered the images. Because speckle noise in the SLC images introduces errors into estimates of flow velocity, we generated a multi-look amplitude image with 2 looks in range and 6 looks in azimuth.

Intensity in the image was then converted to backscattering coefficients. Geometric registration was performed with reference to the existing SAR image database compiled from RADARSAT (Canadian SAR satellite) observations; i.e., the RADARSAT Antarctic Mapping Project (RAMP) image dataset (Jezek and RAMP Product Team, 2002). The RAMP image is characterized by polar stereographic coordinates in the World Geodetic System 1984 (WGS84) reference system. As the present region of concern is of limited extent (90×90 km), we used the pixel coordinates transformed into the Universal Transverse Mercator (UTM) coordinate system. The accuracy of geometric registration was within one pixel, and the resolutions of range and azimuth were 28.0 and 34.8 m, respectively. The obtained Multi-look Geocoded Amplitude (MGA) image is shown in Fig. 2, in which the numbers correspond to the acquired scenes listed in Table 1.

4.2. Calculations of flow velocity

The image correlation method detects similarities in a pair of co-registered images by examining a matched point between the feature window of the reference

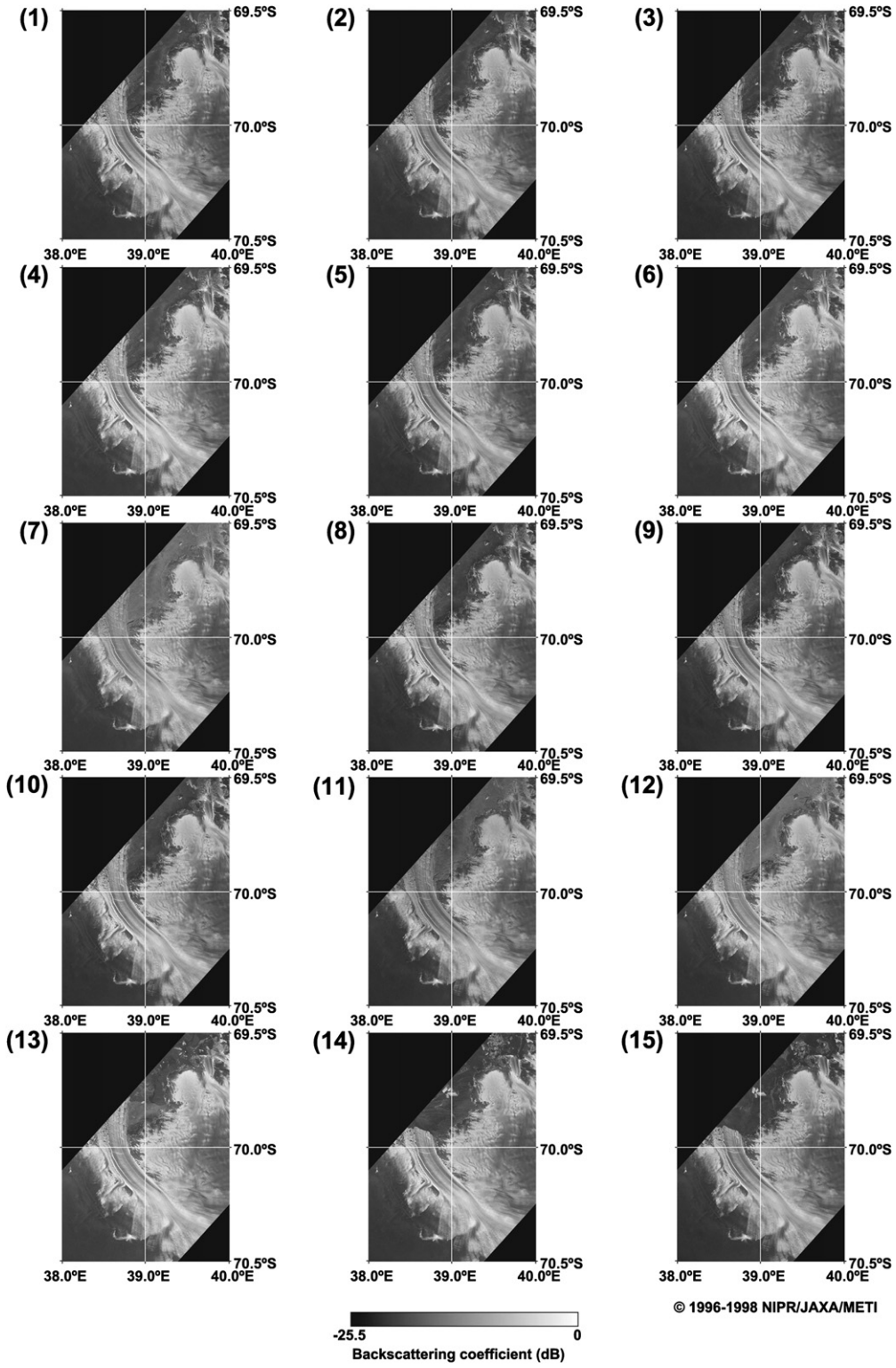

Fig. 2. Multi-look backscatter amplitude images of the JERS-1 SAR scene over Shirase Glacier for the following dates: (1) 30 April 1996, (2) 13 June 1996, (3) 27 July 1996, (4) 9 September 1996, (5) 23 October 1996, (6) 6 December 1996, (7) 19 January 1997, (8) 14 July 1997, (9) 27 August 1997, (10) 10 October 1997, (11) 6 January 1998, (12) 19 February 1998, (13) 4 April 1998, (14) 18 May 1998, (15) 1 July 1998.

(master) image and that in the search (slave) image. In the search procedure, the feature window (with a size of m pixels in azimuth and n pixels in range) was fixed in the master image and tracked within the larger slave image by shifting the central position P of the window (see Fig. 3).

Matching of the two feature windows is a function of range displacement $v - j_0$ and azimuth displacement $u - i_0$ (see Fig. 3), and the degree of similarity of the two windows can be quantified by the following equation:

$$\rho(u,v) = \frac{\sum_i \sum_j [X(i,j) - \overline{X}][Y(i,j) - \overline{Y}]}{\sqrt{\sum_i \sum_j [X(i,j) - \overline{X}]^2} \sqrt{\sum_i \sum_j [Y(i,j) - \overline{Y}]^2}} \quad (1)$$

where $\rho(u,v)$ is the normalized correlation coefficient (from -1 to 1) between the master and slave feature windows at the center location; $X(i, j)$ and $Y(i, j)$ are the intensity values at the range location i and azimuth location j of the master and slave images, respectively; and $\overline{X}$ and $\overline{Y}$ are the average intensity values of the entire master and slave feature windows, respectively.

The size of the feature window was set at $m = 32$ by $n = 32$ pixels with reference to the size of an iceberg at the calving front of Shirase Glacier (size approximately 1 km^2). A matching criterion of acceptance was empirically set at a threshold of correlation coefficient value of 0.20; calculated values in our present case varied from 0.24 to 0.95, with an average of 0.54 for the most probable obtained displacement values (u_p,v_p). After performing the processes described above, we calculated the ice-flow velocity V from the matched features as follows:

$$V = \sqrt{\left[A_s \times (u_p - i_0)\right]^2 + \left[R_s \times (v_p - j_0)\right]^2} \quad (\mathrm{m/44\text{-}days}) \quad (2)$$

where (i_0, j_0) indicates the location of the reference feature window in the master image, and R_s and A_s indicate the spacing of one pixel unit for the range ($R_s = 28.0$ m) and azimuth ($A_s = 34.8$ m) directions, respectively.

The degree of feature mismatch is less than ± 1 pixel unit, corresponding to a mean displacement resolution of ± 36.3 m. This corresponds in turn to an absolute error in ice-flow velocity of ± 36.3 m/44 days $\times$ 365 days $= \pm 0.30$ km/a. The ratio of the absolute error (± 0.30 km/a) to the annual mean velocity at the grounding line (2.33 km/a, as described in Section 5.4), i.e., 0.13, can be considered empirically as the relative error

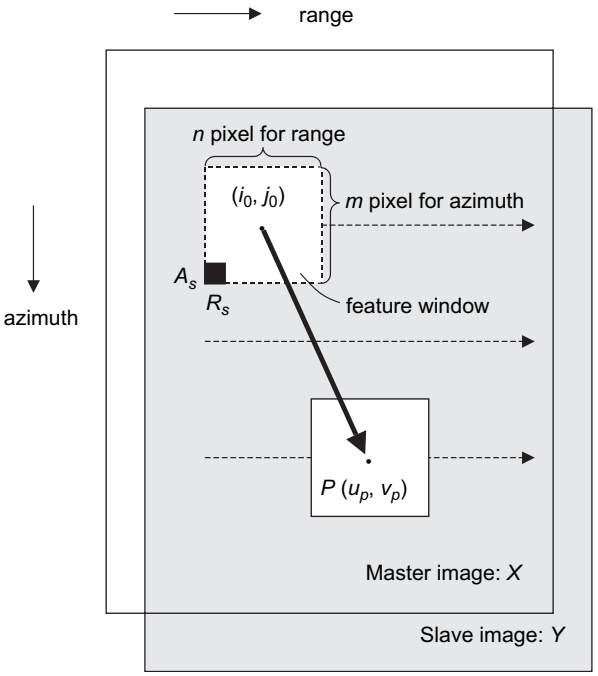

Fig. 3. Schematic diagram illustrating the image correlation method. X and Y indicate the master and slave images, respectively. The square areas in X and Y are $m \times n$ (pixel) windows in the azimuth and range directions, respectively. Matches for these windows were identified using the correlation coefficient ρ, which is given by Eq. (1). When the correlation peak is found at the location (u_p,v_p) on Y, the displacement vector is obtained from $(u_p - i_0, v_p - j_0)$. Consequently, the ice-flow vector can be determined from Eq. (2).

that represents the degree of mismatch of feature displacement. The relative error in ice-flow velocity can then be expressed as ± 0.30 km/a $\times$ 0.13 $= \pm 0.04$ km/a.

The image correlation method was used successfully to determine displacements within the Shirase Glacier region between the successive epochs listed in Table 1. For example, Fig. 4(a) shows the displacement calculated over the 44-day period between 30 April 1996 and 13 June 1996. The flow velocity exceeds 400 m/44-days at the front of the floating ice tongue, while velocity patterns are complex in the upstream region, reflecting the complex pattern of tributary ice streams flowing into the main stream. Similarly, Fig. 4(b)–(l) show the flow velocities calculated for the periods between the other pairs of epochs listed in Table 1.

5. Results and discussion

5.1. Flow-velocity profile

A profile of ice-flow velocity along the central streamline is shown in Fig. 5. The ice-flow velocity

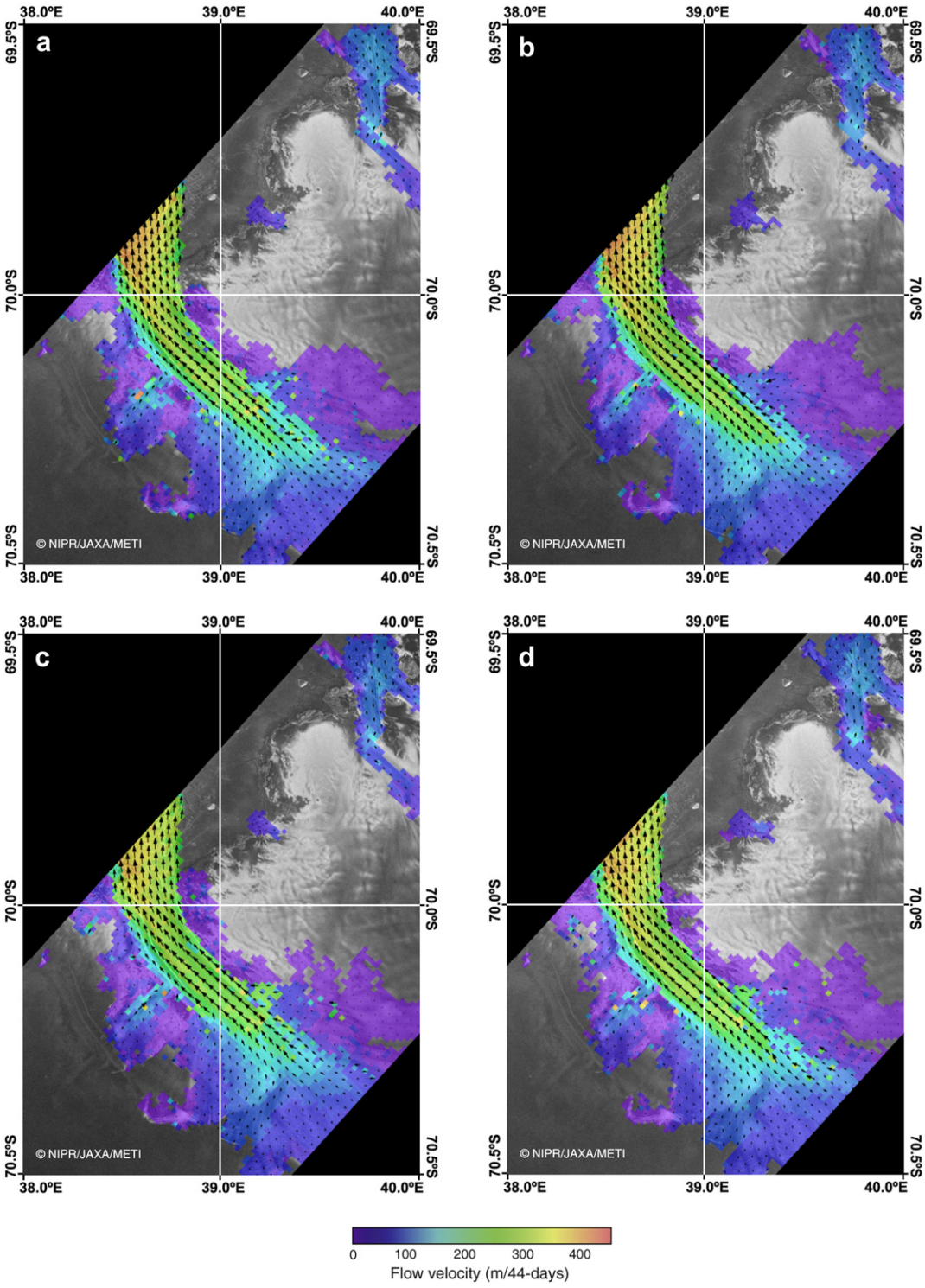

Fig. 4. Color-coded maps of the distribution of ice-flow velocity (m/44-days) within Shirase Glacier, as derived from JERS-1 SAR images and the background in that map used the master image (the first day in epoch). Velocities are calculated based on displacements calculated between the following pairs of images: (a) 30 April and 13 June 1996, (b) 13 June and 27 July 1996, (c) 27 July and 9 September 1996, (d) 9 September and 23 October 1996, (e) 23 October and 6 December 1996, (f) 6 December 1996 and 19 January 1997, (g) 14 July and 27 August 1997, (h) 27 August and 10 October 1997, (i) 6 January and 19 February 1998, (j) 19 February and 4 April 1998, (k) 4 April and 18 May 1998, (l) 18 May and 1 July 1998.

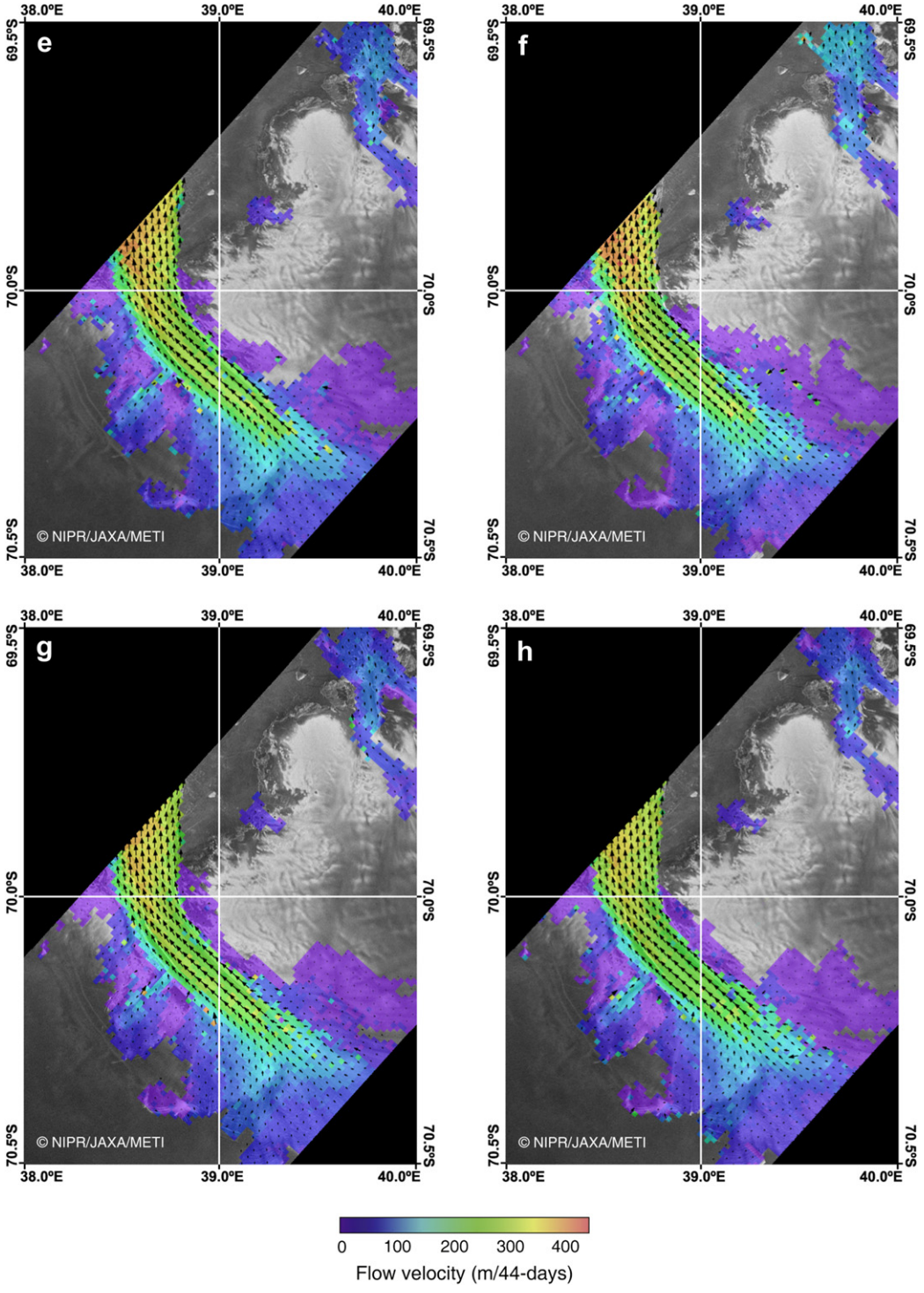

Fig. 4 (*continued*).

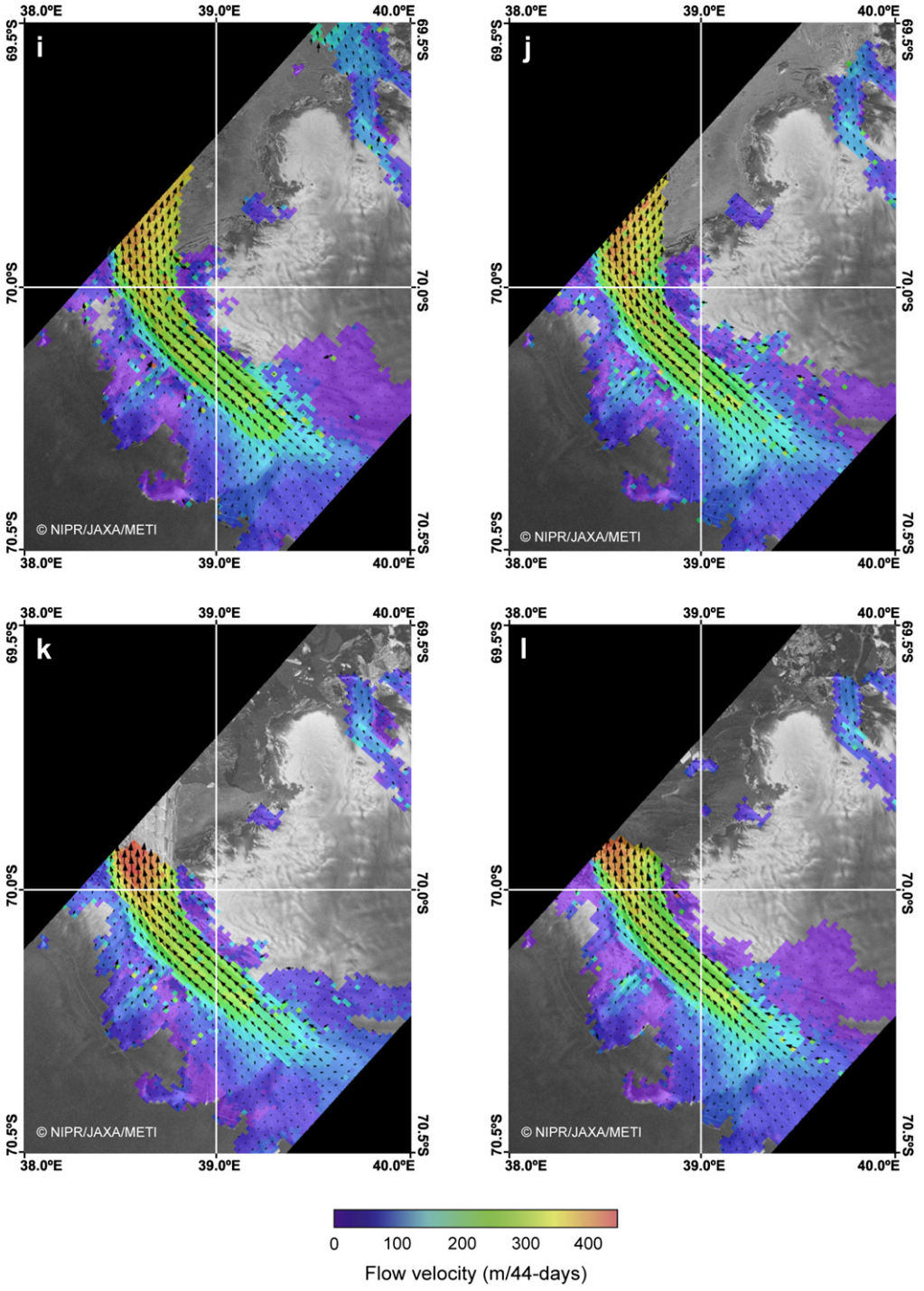

Fig. 4 (*continued*).

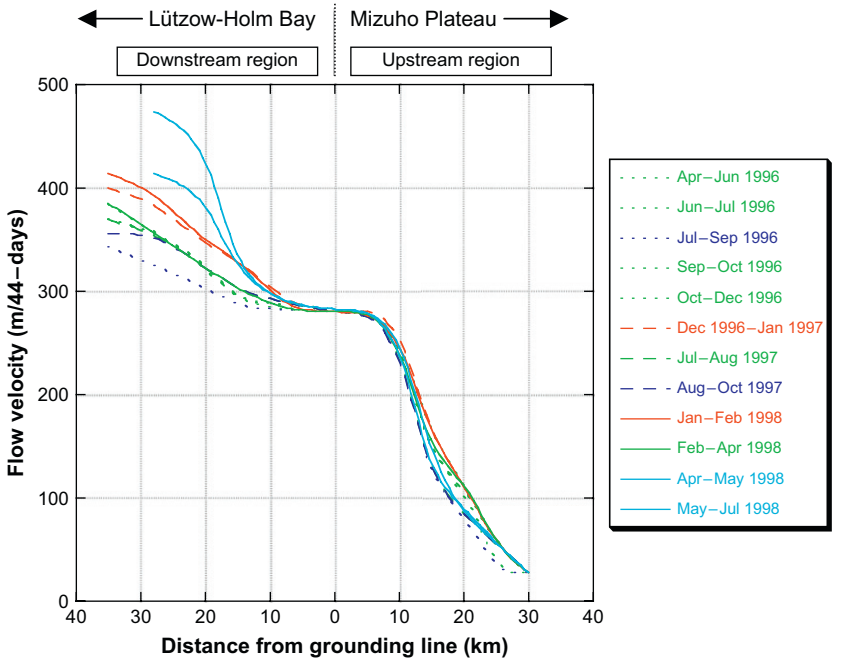

Fig. 5. Profiles of ice flow measured in 1996, 1997, and 1998. Red lines indicate summertime data, while blue lines indicate wintertime data. Light blue lines indicate data calculated following the loss of the floating ice tongue in 1998, and green lines indicate other periods.

increases from the upstream region to the downstream region. The velocity 30 km upstream from the grounding line is 28.0 m/44-days, which corresponds to 0.23 km/a, approximately one-tenth of the velocity at the grounding line.

Mae and Naruse (1978) reported that the fixed-based laminar ice sheet flow with an ice thickness of 3000 m is incapable of generating a surface flow velocity above 0.03 km/a for any reasonable physical properties of ice. The surface flow velocity of 28.0 m/44-days (0.23 km/a) obtained above is approximately 8 times higher than the maximum fixed-base surface flow velocity of the ice layer. The 30-km section of Shirase Glacier located immediately upstream from the grounding line must be wet-based, and an east–west asymmetry in the bedrock topography is believed to give rise to the eastward turning of the glacier, although these hypotheses have yet to be addressed in detail (see Nakamura et al., 2007).

The ice-flow velocity at the grounding line is 280.0 m/44-days, corresponding to 2.32 km/a; this is consistent with the value of 2.3 km/a obtained by Rignot (2002). As illustrated in Fig. 5, the ice-flow velocity at the grounding line is approximately constant for all 12 observed epochs, being devoid of significant seasonal change. The section of grounding zone with a width of 10 km about the grounding line (0 km mark in Fig. 5) may act as a bottleneck, with the narrow trench along this section controlling the velocity of the ice stream in Shirase Glacier.

In contrast to the slightly variable upstream region and approximately constant grounding line, ice-flow velocities in the downstream region are highly variable, depending on both the distance from the grounding line and the observed epoch (season). The highest estimated velocity was 474.3 m/44-days (3.93 km/a) at the terminus of the floating ice tongue, as derived from the image pair taken in April and May of 1998 (Fig. 4(k)). This variability may be related to variability in the extent of sea ice in Lützow-Holm Bay, as discussed in the following sections.

5.2. *Discharge of the floating ice tongue in 1998*

In comparing Fig. 2(13) and (14), it is clear that the floating ice tongue broke away from the glacier at some time between 4 April and 18 May 1998. The size of the lost area of the tongue is estimated to be 198.6 km^2.

Vigorous summertime melting or ice divergence (open-water formation) is occasionally observed in Lützow-Holm Bay. The subsequent breakup of sea ice sometimes results in the southward advance of fractured offshore ice floes into Lützow-Holm Bay, commonly in autumn. According to Ushio (2003), the above

phenomenon has become increasingly pronounced in recent times, and has occurred every year since 1997.

There is a close relation between events involving the break-up of landfast sea ice and the development of embayments. The break-up events are also associated with the enhanced intrusion of oceanic swells into the coastal region during embayment periods (Ushio, 2003). For example, Higashi et al. (1982) reported that ocean swell effects detected in the tidal record at Syowa Station were responsible for the break-up events observed in Lützow-Holm Bay. The results of Ohshima et al. (1996) provide additional evidence that the influence of swell intrusion is enhanced when the wind speed reaches its maximum levels in autumn (April), when the prevailing northeasterly wind is recorded at Syowa Station. After the disintegration of landfast sea ice, the floating ice tongue is easily able to move away under the weak southerly prevailing winds. The combined effect of the sea-ice condition and the autumn wind field may explain the episodic disappearance of the floating ice tongue from Lützow-Holm Bay.

5.3. Seasonal variations in ice flow

In Fig. 5, we define the 1996 summertime as the image pair of December 1996 and January 1997 (dashed red line), while the 1997 summertime is defined as the image pair of January and February 1998 (solid red line). Likewise, we define the 1996 wintertime as the image pair of July and September 1996 (dotted blue line), and the 1997 wintertime as the image pair of August and October 1997 (dashed blue line).

In comparing the red and blue lines, it is clear that the flow velocities are higher in the summertime than in the wintertime. The velocity difference between the 1996 summertime and wintertime was 20.6 m/44-days (0.17 km/a) in the upstream region and 34.7 m/44-days (0.29 km/a) in the downstream region; these values are region-wide averages from the grounding line. In 1997, the corresponding differences were 13.6 and 24.1 m/44-days (0.11 and 0.20 km/a), respectively. Similarly, at the terminus of the floating ice tongue (35 km from the grounding line along the streamline), the velocity difference between the 1996 summertime and wintertime was 56.3 m/44-days (0.47 km/a), while that between the 1997 summertime and wintertime was 58.4 m/44-days (0.48 km/a).

We can summarize the above results as follows: summertime ice-flow velocity in the downstream region shows annual variations (0.3 km/a in 1996 and 0.2 km/a in 1997), whereas flow velocity at the terminus of the floating ice tongue shows an approximately constant summer–winter difference of around 0.47–0.48 km/a.

It is interesting to assess whether the above characteristics are related to meteorological conditions at Syowa Station. The average summertime air temperatures were −0.2 °C in 1996 and −1.3 °C in 1997, while the wintertime values were −14.1 °C in 1996 and −18.3 °C in 1997. Therefore, the summer–winter differences in air temperature were 13.9 °C in 1996 and 17.0 °C in 1997. The large temperature difference observed in 1997 relative to that in 1996 is consistent with the observation of a low ice-flow velocity (0.20 km/a) in 1997 relative to that in 1996 (0.30 km/a). Although a direct relationship has yet to be established between the above air-temperature differences and the stiffness of sea ice, consistent relations have been observed among meteorological observations, sea-ice conditions, and flow velocity in the downstream region of Shirase Glacier. Additional data may help to clarify the characteristics of glacier dynamics in Lützow-Holm Bay.

5.4. Annual variations in ice flow

Table 2 summarizes the calculated annual variations in ice-flow velocity. In combination with the data presented in Fig. 5, it is clear that the ice-flow velocity increases rapidly from the upstream region (1.18 km/a) to the grounding line, where it becomes stagnant at 2.33 km/a before accelerating gradually to 2.62–2.82 km/a in the downstream region and finally 3.05–3.50 km/a at the terminus of the floating ice tongue. In terms of annual variations, most of the obtained values are within the ranges of the associated errors, although the difference between 1997 (3.11 km/a) and 1998 (3.50 km/a) is significant, possibly reflecting an acceleration in ice-flow velocity.

6. Conclusions

We applied an image correlation method to 15 JERS-1 SAR images acquired over the Shirase Glacier

Table 2
Annual mean flow velocity of Shirase Glacier at different regions along the central streamline

Year	Terminus of floating ice tongue	Downstream region	Grounding line	Upstream region
1996	3.05 km/a	2.62 km/a	2.32 km/a	1.17 km/a
1997	3.11 km/a	2.70 km/a	2.32 km/a	1.18 km/a
1998	3.50 km/a	2.82 km/a	2.34 km/a	1.19 km/a

The distance from the grounding line to the upstream and downstream regions was set at 30 km.

region between 30 April 1996 and 1 July 1998. The obtained characteristics of ice-flow velocity along the central streamline are as follows. The velocity increases from the upstream region to the grounding line, where the velocity becomes approximately constant across the 10 km width of the streamline. The velocity increases again from the grounding line towards the floating ice tongue. The velocity is highest in summer and lowest in winter. Among the three annual mean flow velocities (1996, 1997, 1998) determined at the terminus of the floating ice tongue, the highest was recorded in 1998; this appears to be related to the establishment of an outlet between April and May of 1998.

Use of the Phased Array type L-band SAR (PALSAR) sensor onboard the Advanced Land Observing Satellite (ALOS) will reveal the characteristics of the flow velocity of Shirase Glacier in even greater detail.

Acknowledgements

We would like to thank the Japan Meteorological Agency for providing air temperature data recorded at Syowa Station, and the JARE members for their JERS-1 SAR data recorded at Syowa Station. We also thank Dr. T. Yamanokuchi of the Remote Sensing Technology Center of Japan (RESTEC) for his useful discussions regarding this paper. The Ministry of International Trade and Industry (MITI; since reorganized as the Ministry of Economy, Trade and Industry (METI)) and NASDA/JAXA retain ownership of the original JERS-1 data. The JERS-1 SAR scenes employed in this study were archived and analyzed under an agreement between NIPR and JAXA. This research was supported in part by a Grant-in-Aid for Scientific Research (B) 16310015 (P.I. K. Shibuya) by the Japan Society for the Promotion of Science (JSPS).

References

Fujii, Y., 1981. Aerophotographic interpretation of surface features and estimation of ice discharge at the outlet of the Shirase drainage basin, Antarctica. Antarct. Rec. 72, 1−15.

Higashi, A., Goodman, D.J., Kawaguchi, S., Mae, S., 1982. The cause of the breakup of fast ice on March 18, 1980 near Syowa Station, East Antarctica. Mem. Natl. Inst. Polar Res. 24, 222−231 (special issue).

Jezek, K., RAMP Product Team, 2002. RAMP AMM-1 SAR Image Mosaic of Antarctica. Alaska Satellite Facility, Fairbanks, AK, USA.

Mae, S., Naruse, R., 1978. Possible causes of ice sheet thinning in the Mizuho Plateau. Nature 273, 291−292.

Nakawo, M., Ageta, Y., Yoshimura, A., 1978. Discharge of ice across Soya Coast. Mem. Natl. Inst. Polar Res. 7, 235−244 (special issue).

Naruse, R., 1978. Surface flow and strain of the ice sheet measured by a triangulation chain in Mizuho Plateau. Mem. Natl. Inst. Polar Res. 7, 198−226 (special issue).

Nakamura, K., Doi, K., Shibuya, K., 2007. Why is Shirase Glacier turning its flow direction eastward? Polar Sci. 1, 63−71.

Nishio, F., 1990. Ice front fluctuations of Shirase Glacier, East Antarctica. International Conference on the Polar Region in Global Change, Fairbanks, p. 145.

Ohshima, K.I., Takizawa, T., Ushio, S., Kawamura, T., 1996. Seasonal variations of the Antarctica coastal ocean in the vicinity of Lützow-Holm Bay. J. Geophys. Res. 101, (C9), 20617−20628.

Pattyn, F., Derauw, D., 2002. Ice-dynamic conditions of Shirase Glacier, Antarctica, inferred from ERS SAR interferometry. J. Glaciol. 48 (163), 559−565.

Rignot, E., 2002. Mass balance of East Antarctic glaciers and ice shelves from satellite data. Ann. Glaciol 34, 217−227.

Ushio, S., 2003. Frequent sea-ice breakup in Lützow-Holmbukta, Antarctica, based on analysis of ice condition from 1980 to 2003. Antarct. Rec. 47 (3), 338−348.

Ushio, S., Wakabayashi, H., Nishio, F., 2006. Sea ice variation in Lützow-Holmbukta, Antarctica, during the last fifty years. J. Japanese Soc. Snow and Ice 68 (4), 299−305 (in Japanese with English abstract).

Wakabayashi, H., Nishio, F., 2004. Glacier flow estimation by SAR image correlation. Proc. IGARSS. 2, 1136−1139.

Yamanokuchi, T., Doi, K., Shibuya, K., 2005. Validation of grounding line of the East Antarctic ice sheet derived by ERS-1/2 interferometric SAR data. Polar Geosci. 18, 1−14.